Reaction Kinetics, Mechanisms and Catalysis
https://doi.org/10.1007/s11144-024-02681-3

Multifunctional nanoparticles as effective adsorbents for fluoride removal from synthetic and drinking waters: equilibrium, kinetics, and thermodynamics

Nesrine Kamoun[1] · Sahar Raissi[2] · Mohamed Kadri Younes[2] · Hamza Elfil[1]

Received: 2 June 2024 / Accepted: 3 July 2024

Abstract

In this work, a series of bimetallic nano-oxide ZrO_2–CeO_2 xerogel adsorbent with different Ce/Zr molar ratio (0.1, 0.2, 0.3 and 0.5) were prepared in one step via sol–gel method in order to obtain the highest-performing composition for fluoride removal from drinking water. BET, SEM, EDX, TEM, FTIR spectroscopy, and XRD techniques were performed to characterize the solids before and after fluoride adsorption. The selected material exhibits a high surface area ($S_{BET} = 255\ m^2\ g^{-1}$) and a large porosity ($V_P = 0.30\ cm^3\ g^{-1}$). FTIR spectroscopy demonstrated the significant role played by the adjunct sulfate anion and superficial hydroxyl groups in the defluorination process. Thermodynamic study confirms that the sorption is spontaneous and endothermic. Our adsorbent's behavior for the removal of fluoride is described by the Freundlich isotherm model. The pseudo-second order kinetic model represents the adsorption kinetic process. Less than 1 min, 100% of fluoride removal is reached in a wide pH range (2–8). The results of this study were effectively applied to natural drinking water in Tunisia. The development of innovative water treatment technology can be effectively advanced by using our multifunctional nano-oxide.

✉ Nesrine Kamoun
nesrinekamoun22@gmail.com

[1] Lab. Desalination & Natural Water Treatment, Center of Water Research and Technologies, Ecopark of Borj-Cedria, BP 273, 8020 Soliman, Tunisia

[2] Laboratory of Chemistry of Materials and Catalysis, Department of Chemistry, Faculty of Sciences of Tunis, University Tunis El Manar, 2092 Tunis, Tunisia

Published online: 09 August 2024

Graphical abstract

Keywords Functionalized nano-oxide · Multifunctional cerium zirconium · Sol gel · Fluoride adsorption

Introduction

Contamination of drinking water by fluorides is a persistent global and national concern [1]. Thousands of people are exposed to excessive levels of fluoride in water in many countries, especially the phosphate producers like Senegal, Algeria, and Tunisia [2]. In Tunisia, the fluoride content in water from the southern region can reach as high as 3 mg L^{-1}. According to the World Health Organization's 2017 Guidelines for Drinking-Water Quality [3], this level significantly exceeds the drinkability standard, which is set at 1.5 mg L^{-1}. Regular ingestion of such water can engender several diseases, including tooth and bone fluorosis [4]. High concentrations of fluorinated water (> 10 mg L^{-1}) are readily removed by coagulation, precipitation, and other techniques. Nonetheless, low concentrations (less than 10 mg L^{-1}) [5] constitute a persistent problem, hard to solve with those conventional approaches. Numerous treatment techniques, including ion exchange, electrocoagulation, reverse osmosis, electrodialysis, and precipitation, have been adopted [6–8]. However, the limitations of these methods comprise their high cost and low efficiency. Adsorption emerges as one of the most effective, and least expensive technologies for drinking water production. This technology suites the Tunisian context were treatment costs, great flexibility, and straightforward operation are taken into account [9].

Activated carbon is the conventional adsorbent widely used. But this material has high energy requirement in preparation limiting its appeal as an adsorbent [10]. Activated alumina may also be employed. But its minimal threshold for fluoride removal surpassing 2 mg L^{-1} makes it inappropriate for treating drinking water [11]. Several others materials, including silica gel [12], zeolites [13], metal oxides [14], and resins [7], have also been studied in the adsorption process of this mineral. Thanks to their large specific surface area, high porosity, unique physico-chemical properties and good adsorption efficiency, nano-metal oxides have attracted much attention as novel and efficient adsorbents for water treatment [15]. In particular non-toxicity, environmental friendliness, very low water solubility, thermal stability, and high exchange capacity of zirconium oxide makes it an ideal candidate for pollutant removal [16], especially fluoride ions for which zirconium exhibits strong affinity [17].

Nano-rare earth metals including lanthanum, titanium and cerium are also characterized by high affinity to fluoride due to + III and + IV valence state. Among those, CeO_2 shows a significant potential for adsorbing fluoride [18]. Functionalization of metal oxides by oxoanions (SO_4^{2-}, PO_4^{3-}) offers more adsorption active sites at the surface of materials [19, 20]. In particular, sulfate doping enhances significantly the fluoride removal capacity of a variety of adsorbents, including Fe_3O_4/Al_2O_3 [21], Fe–Mg–La metal [22], natroalunite microtubes [19], and hydroxyapatite [23]. Nevertheless, a number of variables, such as temperature, reaction duration, adsorbent

dosage, initial fluoride concentration, solution pH, and reaction time, might influence adsorption efficiency [17].

In this study, we prepare a series of cerium-zirconium xerogel oxide ZrO_2–CeO_2 with different Ce/Zr molar ratio by sol–gel route to be used in the fluoride removal in Tunisian drinking water, Then, the optimum ZrO_2–CeO_2 solid was functionalized by sulfate to enhanced her adsorption capacity.

Reusability study is carried out in order to confirm its sustainable use as a promising adsorbent in the defluoridation of water.

Experimental section

Adsorbent preparation

The sol–gel method was adopted for preparation of our materials. This process is a versatile technique for producing pure mixed oxides with high homogeneity and purity. A sol–gel material's structure changes gradually as a result of several hydrolysis–condensation processes. The method outlined by Ksila et al. [24] describes the mechanism of the gel formation from but-oxide zirconium $(BuO)_4Zr$ precursor to undergo sequential hydrolysis and condensation processes.

Zirconium butoxide $Zr(OBu)_4$ (Aldrich 80% in 1-butanol) is dissolved in 1-butanol (Aldrich, 99%) followed by addition of quantity of nitric acid HNO_3 (Aldrich, 65%) with a molar ratio $nHNO_3/nZr = 0.5$. $(NH_4)_2$ $[Ce(NO_3)_6]$ (Aldrich, 99.9%) is then added with different molar ratio Ce/Zr = 0.1, 0.2, 0.3 and 0.5. Finally, water is slowly adjunct with ratio $n(H_2O)/n(Zr) = 3$ to ensure gelling. The wet gel is dried by simple evaporation at temperature = 110 °C for 24 h to obtain nano-oxide ZrO_2–CeO_2 materials. To determine the optimum composite, these prepared materials are tested in the fluoride removal. Then, the optimal material is functionalized by sulfate, by addition of concentrated H_2SO_4 (Acros, 98%) with molar ratio S/Zr = 0.5 before the gelling step to obtained multifunctional nano-oxide SO_4^{2-}–ZrO_2–CeO_2 material named XSZC.

Adsorbent characterization

Textural characterization is achieved using a computer-based AST-derived Micromeritics device (type ASAP 2000). The samples are first degassed under vacuum at 473 K for 4 h. The specific surface area and pore size distribution are determined using the BET and BJH methods.

XRD patterns are realized on an automatic Philips Panalytical diffractometer using Cu K_α radiation ($\lambda = 1.5412$ Å) and nickel monochromator. Reticular distances calculated are compared to those given by the Joint Committee on Powder Diffraction Standards.

Fourier transform infrared spectroscopy (FTIR) spectra of the samples diluted in KBr are recorded with a SHIMADZU, IR Affinity-1 spectrometer over a range of 4000–400 cm^{-1} in the transmission mode.

Material morphological structure before and after fluoride removal are achieved using an Ultra-high-Resolution Analytical Electron Microscope (HR-FESEM Hitachi SU-70).

For TEM observations, samples are dispersed in ethanol by applying the ultrasonic wave and are collected on a holly micro-grid supported on a copper grid mesh. An emission field type TEM (JEOL JEM2010F) operated at 200 kV is used for the observations. The chemical compositions of the synthesized samples are confirmed by energy dispersive X-ray spectroscopic analysis (EDX) using an X-ray detector attached to the TEM instrument.

The pH at the point of zero charge (pHpzc) of the nano-oxide is established by batch equilibration technique. In many flasks, 20 mL of 0.1 M NaCl is added to each flask and initial pH is adjusted from 2 to 10 with dilute HCl (0.1 M) and NaOH (0.1 M) solutions. To each flask, 50 mg of the adsorbent is added. The solutions are agitated for 24 h. The final pH is measured after filtering the solution.

Batch adsorption experiments

Defluoridation experiments were performed by mixing the adsorbent with fixed volume (20 mL) of fluoride solution (NaF solution of initial concentration varying from 2 to 10 mg L^{-1} (batch adsorption technique). All adsorption experiments are carried out using a magnetic Multistirrer VELP scientifica with a stirring speed of 300 rpm. The solution is then filtered by filter paper with 45 µm of porosity. By means of fluoride ion selective electrode (ISE model no. 6.0502.150, Metrohm Switzerland) the fluoride ion concentration, before and after adsorption, is determined. The ion-meter is calibrated before every use. The detection limit is 20 µg L^{-1}.

The percent removal (%) and the adsorption capacity (mg g^{-1}) are calculated using Eqs. 1 and 2:

$$\%\text{Removal} = \frac{c_0 - c_e}{c_0} \times 100 \tag{1}$$

$$q_e = \frac{(c_0 - c_e)\,V}{m} \tag{2}$$

here c_0 and c_e are the initial and equilibrium liquid phase concentrations in mg L^{-1} of fluoride, q_e is the adsorption capacity (mg g^{-1}), m is the mass of the adsorbent (g). V is the volume of the solution (L). All adsorption experiences were carried out in triplicate, by generating three repeat treated solutions at every chosen condition. Adsorption experiences are plotted as the average %fluoride removal sorbed for each triplicate and error bars are calculated as the standard deviation of the three repeat samples.

Adsorption isotherms

A set volume (20 mL) of fluoride solution at various concentrations of 2–5 and 10 mg L^{-1} is mixed with 30 mg of SO_4^{2-}–ZrO_2–CeO_2 adsorbent to conduct an adsorption isotherm experiment. The determination of the adsorption model is carried out by examining the interaction between the fluoride and nano-oxide SO_4^{2-}–ZrO_2–CeO_2 adsorbent using the nonlinear Langmuir and Freundlich models, whose equations are presented in Table 7 [25] In this context, nonlinear models are utilized using excel solver [26].

Adsorption kinetics

To predict the mechanism of fluoride adsorption by nano-oxide SO_4^{2-}–ZrO_2–CeO_2 adsorbent, two nonlinear kinetic models are verified, namely the pseudo-first order and the pseudo-second order, whose equations are presented in Table 5 [27]. In this context, nonlinear models are utilized using excel solver [26].

Error analysis

To validate the adsorption system model, an error analysis including three error functions is carried out on the data. Those functions are the mean square residue (MSR) in Eq. 3, the coefficient of determination (R^2) in Eq. 4 and the Chi-square (χ^2) in Eq. 5. The best-fitting model of nonlinear models based on the value of error functions is that R^2 has the highest value closer to the unit, with minimum values of χ^2 and MRS.

$$\mathrm{MSR} = \frac{\sum_{i=1}^{n}(q_{e,exp} - q_{e,calc})^2}{n - p} \tag{3}$$

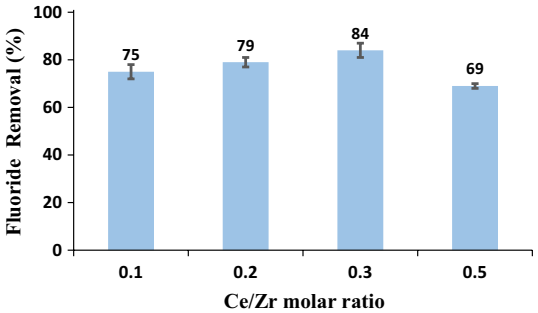

Fig. 1 Effect of molar ratio (Ce/Zr) on the bimetallic nano-oxide ZrO_2–CeO_2 adsorbent on the fluoride removal. Experimental conditions: $[F^-] = 5$ mg L^{-1}, pH 7, Contact time = 5 min, Temperature (T = 25 °C), adsorbent dose m = 30 mg, Volume V = 20 mL, stirring speed = 300 rpm). Error bars are calculated as the standard deviation % fluoride sorbed of triplicate data sets

$$R^2 = 1 - \frac{\sum_{i=1}^{n}(q_{e,exp} - q_{e,calc})^2}{\sum_{i=1}^{n}(q_{e,exp} - \overline{q_{exp}})^2} \tag{4}$$

$$\chi 2 = \frac{\sum_{i=1}^{n}(q_{e,exp} - q_{e,calc})^2}{q_{e,calc}} \tag{5}$$

here $q_{e,exp}$ is the equilibrium amount of adsorbate obtained from experiment (mg g^{-1}), $q_{e,calc}$ is the equilibrium capacity obtained from isotherm model (mg g^{-1}), and n is the number of observations in the experimental data.

Results and discussion

Adsorbents optimization: effect of cerium content

Adsorbent optimization tests are performed to obtain the highest performing composition of ZrO_2–CeO_2 (XZC) for the removal of F^- ions. As seen in Fig. 1, the adsorption efficiency is significantly impacted by the Ce/Zr molar ratio. The highest sorption effectiveness (84%) for the bimetal nano-oxide XZC is obtained at molar ratio of 0.3. Therefore, the optimized ZrO_2–CeO_2 material is selected to be functionalized by sulfate groups to obtain the multifunctional nano-oxide SO_4^{2-}–ZrO_2–CeO_2 xerogel adsorbent which is named XSZC. The multifunctional nanoparticular XSZC

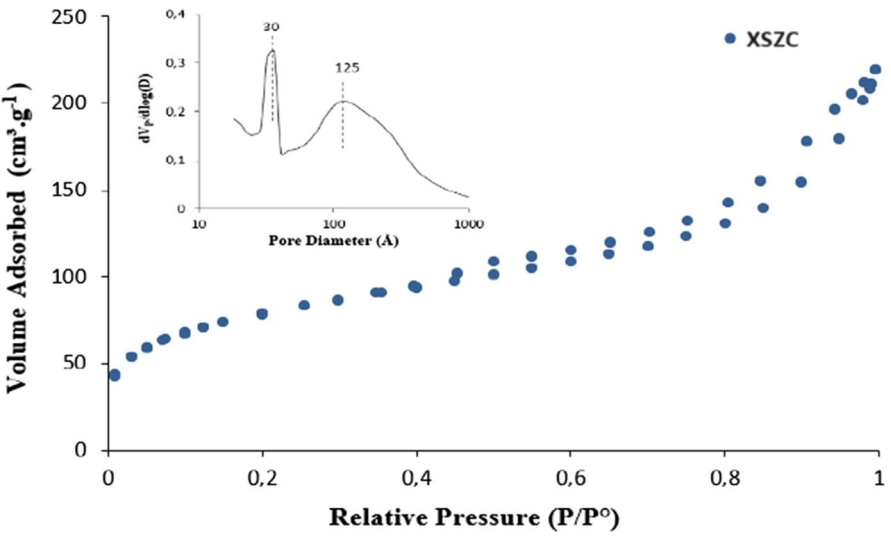

Fig. 2 Adsorption–desorption isotherm and BJH pore distribution of multifunctional nano-oxide SO_4^{2-}–ZrO_2–CeO_2 adsorbent before fluoride removal (XSZC)

material is characterized before and after fluoride adsorption using BET, SEM, EDX, TEM, FTIR spectroscopy and XRD techniques.

Characterization of SO_4^{2-}–ZrO_2–CeO_2

Textural properties

N_2 adsorption–desorption isotherms play a key role in the explanation of textural properties of materials mainly used as adsorbent.

The isotherms at 77 K and pore size distribution curves, determined by BJH method, of XSZC sample before and after fluoride adsorption are illustrated in Figs. 2 and S1. The observed isotherms of fresh adsorbent is of type IV (b), typical of mesoporous materials [28]. Hysteresis loops is of type H3 indicating the presence of broad pores resulting from texture in layers [28]. Recently, considering their large specific area and developed texture, mesoporous materials emerge as excellent adsorbents, more appropriate than macroporous and microporous materials for effective removal of pollutants [29].

BJH curve of this material indicate large pore size distribution around 125 Å. We also note the presence of a peak situated at about 30 Å, considered as a phantom peak due to various phenomena. This peak appears when capillary forces and gas adsorption within extremely small holes prevent the pores from being completely emptied during the desorption process. As the pressure decreases, some of the gas is trapped inside these tiny pores.

The xerogel nano-oxide's porosity features a complex pore structure with different sizes of pores. The variety of pore types and their large size dispersion engender pores' connectivity and sample's internal tension strength.

This discrepancy can be mainly explained by the xerogels-related phenomenon of pore shrinkage, which is caused by surface tension forces, solvent evaporation, and capillary forces.

Atmospheric solvent evaporation creates a surface tension that increases capillary forces and causes the pore walls to constrict when a contact between the solvent and the air inside the pore forms. This result, in the compression of the pore structure, lowers the pore volume and densifies the xerogel material as a whole [20]. Our multifunctional nano-oxide XSZC adsorbent presents pores larger than F^- ions diameter (1.33 Å), indicating their easy insertion.

Table 1 displays the textural characteristics of the adsorbents. The multifunctional nano-oxide XSZC has a significant porosity ($V_P = 0.30$ cm^3 g^{-1}) and a high

Table 1 Textural properties of prepared solids: SO_4^{2-}–ZrO_2–CeO_2 (XSZC (before adsorption)), SO_4^{2-}–ZrO_2–CeO_2–F (XSZC-F (after adsorption)), ZrO_2–CeO_2 (XZC)

Adsorbents	S_{BET} (m^2 g^{-1})	V_p (cm^3 g^{-1})	D_p (Å)
XSZC	255	0.30	30–125
XSZC-F	9	0.024	36–65–101–200
XZC	274	0.45	36–157

Table 2 Element weight percentage of multifunctional nano-oxide SO_4^{2-}–ZrO_2–CeO_2 (XSZC) before and after fluoride adsorption

XSZC	C	O	Ce	Zr	S	F	Total amount
Weight percentage (%)							
Before adsorption	8.59	32.14	10.11	41.29	7.87	0	100
After adsorption	13.28	29.21	9.98	40.97	4.58	1.98	100

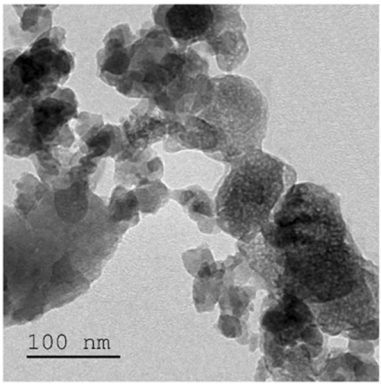

Fig. 3 TEM images of multifunctional nano-oxide SO_4^{2-}–ZrO_2–CeO_2 adsorbent

surface area (S_{BET} = 255 m^2 g^{-1}). This outcome highlights an appropriate choice of the one-step sol–gel process as a preparation technique, in order to produce an adsorbent with a developed texture. Large specific surface area, in fact, is known to imply more exposed active sites on the solid surface, which can enhance fluoride adsorption efficacy [29]. Furthermore, the synthesis of these oxides with an abundance of hydroxyl groups appears to be a desirable outcome of the sol–gel method.

Moreover, it has been noted [30] that the hydrolysis reaction of metallic oxides with water produces hydroxyl groups on the surface of the solid, which are thought to be active sites for the adsorption of the water's anions [31].

After fluoride adsorption, the nano-oxide material loses its porosity and the isotherm of N_2 adsorption–desorption isotherm fits type II, characteristic of non porous materials with persistence of hysteresis loop H3 due to the presence of some mesoporous. We observe a considerable decrease in the pore volume (from 0.30 to 0.024 cm^3 g^{-1}) and surface area (approximately 96% less than fresh XSZC) of XSZC-F, indicating that F^- insertion saturated the pores between the layers of the nano-oxide adsorbent. The analysis of the BJH desorption pore-size distribution of used adsorbent shows a polymodal distribution shifted towards large pore diameters.

SEM, EDS and TEM analysis

Fig. S2 displays the XZCS material's scanning electron microscopy micrographs before and after the fluoride removal process. The XZCS micrograph (Fig. S2a) demonstrates how the adsorbent's surface is heterogeneous, with numerous cavities

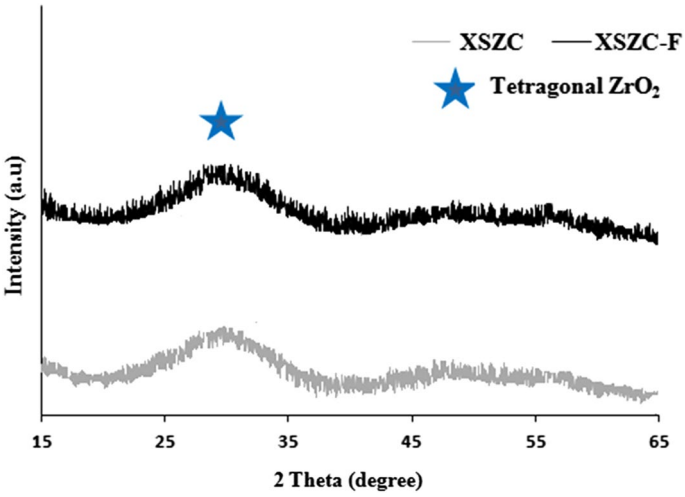

Fig. 4 XRD patterns of multifunctional nano-oxide SO_4^{2-}–ZrO_2–CeO_2 adsorbent: **a** before fluoride removal (XSZC), **b** after fluoride removal (XSZC-F)

that have a diameter of roughly 4 µm and irregular forms. On the other hand, fluoride deposition on the material surface is visible in the SEM of the fluoride adsorbed solid XZCS-F (Fig. S2b) which is confirmed by EDS study.

Table 2 and Fig. S2c provide an EDS study of the multifunctional nano-oxide adsorbent's composition before and after fluoride adsorption. In the fresh solid, it is found that O (32.14%), Ce (10.11%), Zr (41.29%), and S (7.87%) are the primary compensatory elements. Following fluoride adsorption (Fig. S2d), a fluoride peak with 1.98% emerged, confirming fluoride adsorption. Additionally, following adsorption, the amount of O and S elements is reduced, indicating that some Zr–OH, Ce–OH, and SO_4^{2-} exchanged with fluoride ions [32].

TEM analysis of multifunctional nano-oxide adsorbent (Fig. 3) shows that XSZC is characterized by spherical nanoparticule aggregates with diameter of about10 nm.

XRD analysis

The multifunctional nano-oxide's X-ray diffraction (XRD) patterns are displayed in Fig. 4 before and after fluoride adsorption. The produced solid has an almost amorphous structure with a broad peak centered at $2\theta = 30°$, indicating a poorly developed tetragonal ZrO_2 phase (JCPDS 17-0923). Patel et al. [31] reported a similar outcome. The produced material's amorphous form may improve the adsorbent's accessibility to fluoride. Amorphous materials are shown to have more active spots on their surfaces [33]. Following fluoride adsorption, the distinctive peaks of tetragonal zirconia are not altered and any more peaks related to the formation of ZrF_4 or $NaZrF_5$ are detected, as in the case of other works [34] (Fig. 4).

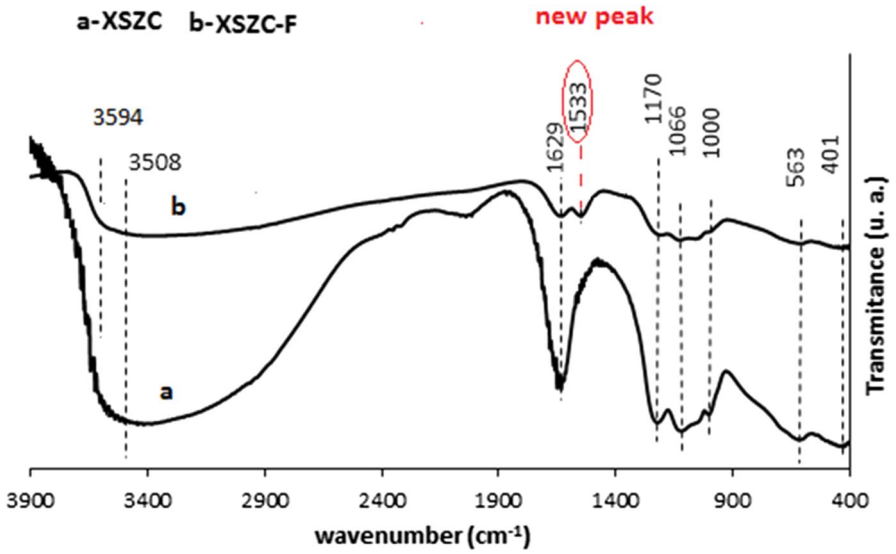

Fig. 5 IR spectra of multifunctional nano-oxide SO_4^{2-}–ZrO_2–CeO_2 adsorbent: **a** before fluoride removal (XSZC), **b** after fluoride removal (XSZC-F)

pH_{PZC}

The pH_{PZC} is an important parameter in adsorption process, especially when electrostatic interactions are involved. It determinates the adsorbent's surface charge. The pH_{PZC} of the multifunctional nano-oxide material (Fig. S3) is around 5.4. When the pH of the nano-oxide nanoparticle is inferior to 5.4, the surface is positively charged. When the pH surpasses this value is more than pH_{PZC}, it becomes negatively charged.

FTIR analysis and possible adsorption mechanism of fluoride onto SO_4^{2-}–ZrO_2–CeO_2 adsorbent

FTIR spectra of nano-oxide SO_4^{2-}–ZrO_2–CeO_2 material before and after fluoride adsorption are shown in Fig. 5.

The XZCS spectra (line a) shows a fine peak at 1629 cm^{-1}, indicative of non-dissociated water molecules (δ_{HOH}) and a wide peak centered at 3508 cm^{-1}, attributed to the stretching vibration of the hydroxyl group (Zr-OH and/or Ce-OH) [32, 35]. The Zr–O and/or Ce–O bond is related to the bands seen at 401 and 563 cm^{-1}36. Sulfate groups engender a multiplicity of bands in the 1000–1200 cm^{-1} area, specifically at 1000, 1066, and 1170 cm^{-1}. These bands are linked to both symmetric and asymmetric stretching frequencies of S–O and S–O bonds [36].

After fluoride adsorption, we observe a shift of hydroxyl peak from 3508 to 3594 cm^{-1} indicating the participation of the surface hydroxyl groups in the fluoride adsorption process. Furthermore, following fluoride adsorption, the intensity of the band at 1629 cm^{-1}, diminishes as a result of F^- exchange with –OH groups on the

surface of adsorbents [34]. This finding indicates a significant replacement of the surface hydroxyl groups by fluoride.

The intensity of sulfate groups peak is also affected after F^- adsorption. This significant decrease is due to the F^- exchange with SO_4^{2-} [37].

FTIR data confirms the contribution of both hydroxyl groups and sulfate anions to the ion-exchange fluoride adsorption process. Additionally, we note the appearance of a new peak at 1533 cm^{-1}, attributed to $[HF_2]^-$ group [34] which confirmed the presence of F^- on the surface of XSZC adsorbent after fluoride adsorption.

The possible adsorption mechanism of fluoride onto nano-oxide SO_4^{2-}–ZrO_2–CeO_2 adsorbent can describe as follows:

When the pH falls below pH_{PZC}, the adsorbent's surface becomes positively charged. Fluoride is adsorbed onto nano-oxide SO_4^{2-}–ZrO_2–CeO_2 surface through a strong electrostatic attraction between the adsorbent's positive surface charge and the fluoride anion. Anionic exchange (between the hydroxyl or sulfate groups in the adsorbent and the fluoride in the solution is another possible pathway for the adsorption mechanism of fluoride.

At pH superior to pH_{PZC}, the adsorbent's negatively charged surface exerts a repulsive force on the fluoride anion. Ion exchange (between the hydroxyl or sulfate groups in the adsorbent and the fluoride in the solution) is the only way explaining fluoride trapping on the solid phase.

In conclusion, the development of a new peak at 1533 cm^{-1}, characteristic of $[HF_2]^-$ group, during the FTIR analysis of the adsorbent following fluoride removal confirms the ionic exchange between fluoride and both OH^- and SO_4^{2-} groups. On the other hand, the significant drop in BET surface and porous volume upon adsorption indicates that fluoride has been incorporated onto pores. These findings demonstrated both chemical and physical sorption phenomena.

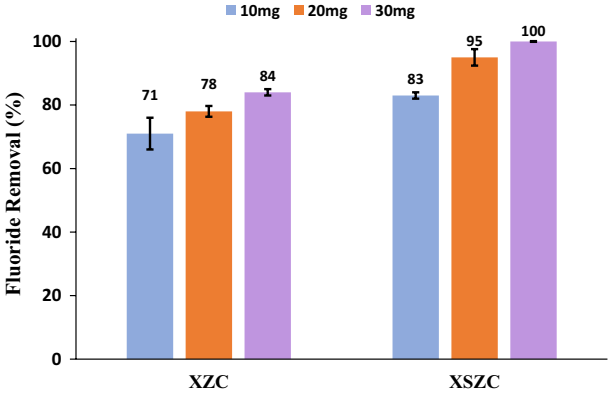

Fig. 6 Effect of addition of sulfate ions on the bimetallic nano-oxide ZrO_2–CeO_2 adsorbent on the fluoride removal: XZC (without sulfate), XSZC (with sulfate). Experimental conditions: $[F^-] = 5$ mg L^{-1}, pH 7, Contact time = 5 min, Temperature (T = 25 °C), stirring speed = 300 rpm. Error bars are calculated as the standard deviation % fluoride sorbed of triplicate data sets. Y axis error bars are not visible where the standard deviation in % fluoride sorbed is < 1%

Table 3 Attribution of IR bands of different adsorbents: SO_4^{2-}–ZrO_2–CeO_2 (XSZC) and ZrO_2–CeO_2 (XZC)

Functional group	–OH	δ_{HOH}	Zr–OH	ν_{S-O} in SO_4^{2-}	$(\delta_{SO})_{as}$ in SO_4^{2-}	ZrO_2
Adsorbents			Frequency (cm^{-1})			
XZC	3465	1629	1384	–	–	420–513
XSZC	3508	1629	–	1000–1170	1066	401–563

Effect of the functionalization of the optimized ZrO_2–CeO_2 xerogel adsorbent by sulfate ions

The impact of sulfate groups addition to ZrO_2–CeO_2 on fluoride adsorption is displayed in Fig. 6. The results demonstrate that, for a range of mass (10–30 mg), the SO_4^{2-}–ZrO_2–CeO_2 adsorbent (XSZC) exhibits significantly more fluoride adsorption than the optimized ZrO_2–CeO_2 (XZC). This suggests that sulfate doping is important for the fluoride adsorption process, generating a new type of active sites formed of sulfate. It is commonly known that solids with Lewis and Brønsted acidity are created when sulfate groups functionalize zirconia. Fluoride ions, as Lewis base, have good affinity to those produced sites.

Compared to non-functionalized adsorbent (84%), the XSZC adsorbent exhibits the best removal rate of around 100% at an adsorbent dose of 30 mg. The solid's evolved texture is responsible for this outcome. The large specific surface area (more than 200 $m^2\ g^{-1}$) and mesoporous structure with various types of pores expose a large number of available active sites. In addition, the simultaneous presence of superficial hydroxyl groups and sulfate anions enhance greatly the fluoride removal performance of cerium-zirconium oxide adsorbent, through an availability of multiple adsorption active sites with good affinity towards fluoride in solution.

For the fluoride adsorption process, the presence of additional sulfate active groups (Table 3) may be more significant than the slight decrease in adsorbent surface area (255 $m^2\ g^{-1}$) of XSZC compared to XZC (274 $m^2\ g^{-1}$) (Table 1).

According to Chai et al. [21], sulfate addition to Fe_3O_4/Al_2O_3 nanoparticles increases the fluoride adsorption effectiveness. The same phenomenon is reported by Chen et al. [23]. Sulfate added to hydroxyapatite (HAP) enhances the ion-exchange-based fluoride removal capabilities of HPA adsorbent.

Optimization of the adsorption parameters

Effect of adsorbent dose

The optimization of fluoride adsorption conditions is performed on our multifunctional nano-oxide SO_4^{2-}–ZrO_2–CeO_2.

The effect of adsorbent dose (Fig. S4) is studied by varying the mass of XZCS from 10 to 50 mg. The surge of adsorbent dose from 10 to 30 mg increases the removal percentage of fluoride from 83 to 100%, thanks to the availability of

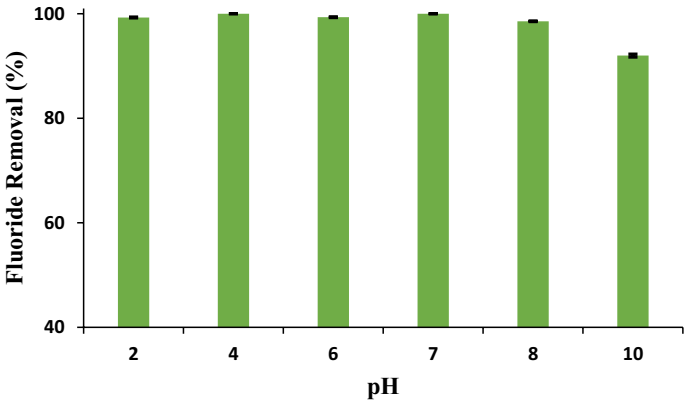

Fig. 7 Effect of pH on the fluoride removal by SO_4^{2-}–ZrO_2–CeO_2 adsorbent. Experimental conditions: $[F^-]=5$ mg L^{-1}, adsorbent dose = 30 mg, contact time = 5 min, temperature (T = 25 °C), stirring speed = 300 rpm. Error bars are calculated as the standard deviation % fluoride sorbed of triplicate data sets. In all cases Y axis error bars are not visible where the standard deviation in % fluoride sorbed is < 1%

adsorption sites for interaction with the F^- anion. When the dose of XZCS reaches 30 mg, the clearance percentage stays practically constant. As a result, a 30 mg adsorbent dose was used for next experiments.

Effect of pH

One of the main factors influencing the adsorbent-anion interaction is pH. It has a great impact on both the adsorption process and the adsorbents' surface charges. The effect of pH on fluoride adsorption is achieved in a pH range between 2 and 11 (Fig. 7). The maximum removal percentage of fluoride is observed in the wide initial pH ranging from 2 to 8, which is advantageous for many types of water. Most adsorbents require a pH adjustment in the range 5 to 6 to ensure fluoride removal from drinking water. This characteristic offers our adsorbent a significant edge over widely used ones [30].

In the acidic environment, at $pH < pH_{PZC}$, active sites of our nano-oxide are protonated and lead to the formation of MOH^{2+} on the surface of the solid. The fluoride anions are strongly attracted to such positive charges. Korde et al. [29] confirm a similar outcome.

Electrostatic attraction is the fundamental basis of the fluoride adsorption mechanism in those conditions. At pH > PHpzc, the surface becomes negatively charged (Fig. S3). However, the solid preserves its adsorption capacity, until pH 8. This high performance, which defies repulsion forces, can be explained by an anion exchange mechanism.

At pH > 8, percentage of fluoride removal decreases slightly. This reduction in alkaline pH can be explained by a competition between the hydroxyl ions from the alkaline environment and fluoride ions, for the active sites on the nano-oxide SO_4^{2-}–ZrO_2–CeO_2 adsorbent. Electrostatic repulsion between negative surface

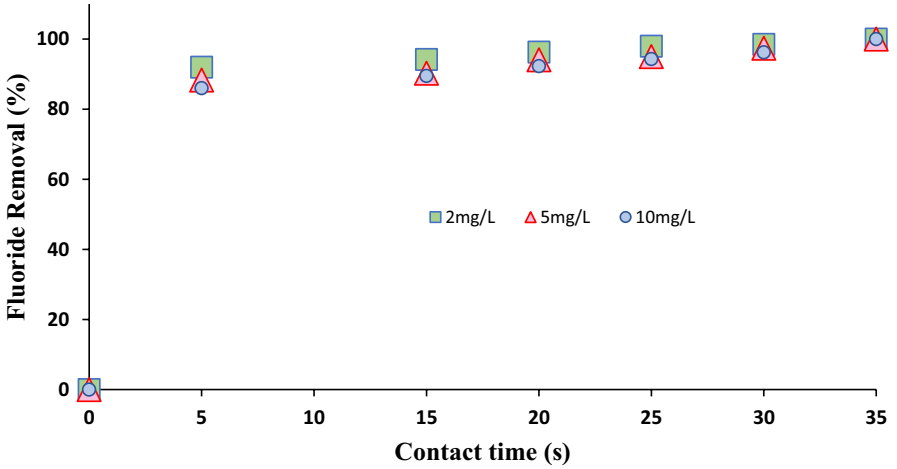

Fig. 8 Effect of contact time on the fluoride removal by SO_4^{2-}–ZrO_2–CeO_2 adsorbent. Experimental conditions: $[F^-] = 5$ mg L^{-1}, adsorbent dose = 30 mg, pH 7, contact time = 35 s, temperature (T = 25 °C), stirring speed = 300 rpm. Error bars are calculated as the standard deviation % fluoride sorbed of triplicate data sets. In all cases, Y axis error bars are not visible where the standard deviation in % fluoride sorbed is < 1%

charge of adsorbent (Fig. S3) and F^- in solution, can also justify the decrease of our adsorbent performances.

Effect of contact time and initial fluoride concentration

Fig. 8 shows the impact of contact times between 0 and 35 s on the fluoride adsorption at three initial concentrations (2, 5, and 10 mg L^{-1}). It is evident that adsorption occurs at a very rapid rate, at the beginning of the adsorption process (0–5 s). The availability of active sites of our multifunctional nano-oxide justifies the solid's affinity for the fluoride ion. After 5 s, the rate of adsorption removal becomes practically constant since almost the totality of remaining fluoride is immediately trapped by the solid phase. The adsorption process is not affected by the initial concentration of fluoride ions, which is a great advantage allowing the possibility of working with different types of drinking water. The contact time of 35 s is chosen for the next steps. The rapid extraction kinetic of the SO_4^{2-}–ZrO_2–CeO_2 solid (contact time at equilibrium < 1 min) makes this material among the top adsorbents currently known in fluoride removal. This rapid extraction kinetics is attributed to fast and short diffusion path associated to the nano- scale of our bimetallic oxide [38]. Like our study, a number of zirconium-modified materials exhibit near-total fluoride elimination in a relatively short amount of time. Iron (III)–zirconium (IV) is used by Swain et al. [39] to remove 90% of the fluoride from a solution containing 5–25 ppm in 45 min. Dou et al. [40] employ mesostructured zirconium phosphate to remove 96% of the fluoride from a 10 ppm solution in 15 min. However, our multifunctional nano-oxide

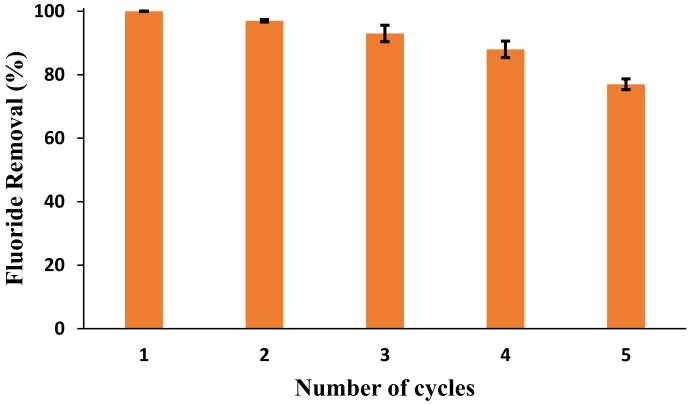

Fig. 9 Efficiency of regenerated SO_4^{2-}–ZrO_2–CeO_2 material removal. Experimental conditions: adsorbent dose = 30 mg; pH 7; contact time = 35 s; temperature (T = 25 °C), stirring speed = 300 rpm. Error bars are calculated as the standard deviation % fluoride sorbed of triplicate data sets. In all cases Y axis error bars are not visible where the standard deviation in % fluoride sorbed is < 1%

outperforms them with its remarkable fluoride removal speed. It is to note that many proposed processes [34, 41–43] require more much time (many hours) to reach fluoride standard of drinking water.

Effect of temperature

The temperature affects the adsorption process. By rising from 5 to 25 °C, the removal rate of the adsorbent increases from 81 to 100% (Fig. S5). This outcome verifies the endothermic nature of the adsorption process. No discernible difference from 25 to 45 °C occurred after that.

Regenerations and reusability study

One of the key factors for the possible commercial application of our multifunctional nano-oxide is its regeneration and reusability. Regeneration experiments using NaOH at various concentrations (1 M, 2 M, and 3 M) are conducted to examine the sorbent's reusability (Fig. S6). After regeneration by NaOH (3 M), the best fluoride removal rate of adsorbent is achieved. Studies using the regenerate adsorbent for five consecutive cycles (Fig. 9) demonstrate that the adsorption capacity in cycles 2 and 3 is as high as 97% and 93%, respectively, of that seen in cycle 1. The adsorption capacity of F^- is 77% of its initial value after five cycles. This result implies a promising multicycle reuse potential of our adsorbent.

Table 4 Thermodynamics parameters for F^- adsorption onto multifunctional nano-oxide SO_4^{2-}–ZrO_2–CeO_2 adsorbent

ΔH° (kJ mol^{-1})	ΔS° (J mol^{-1} K^{-1})	ΔG° (kJ mol^{-1})	
59.91 ± 10	239 ± 34	278 K	6.53 ± 2.4
		283 K	− 7.72 ± 2.4
		288 K	− 8.92 ± 2.4
		298 K	− 11.31 ± 2.4
		308 K	− 13.70 ± 2.4
		318 K	− 16.09 ± 2.4

Thermodynamic study

Adsorption thermodynamics is studied to ascertain the spontaneity and feasibility of the adsorption process. The standard enthalpy change ($\Delta_r H°$), the standard entropy change ($\Delta_r S°$), and the standard Gibbs free energy change ($\Delta_r G°$) are among the thermodynamic parameters that can be computed using Eqs. 6, 7, and 8.

$$\Delta G° = -RT\ln K_d = \Delta H° - T\Delta S° \tag{6}$$

$$K_d = \frac{qe}{Ce} \tag{7}$$

Table 5 Parameters and error functions data for various kinetic model for the adsorption of fluoride onto the multifunctional nano-oxide SO_4^{2-}–ZrO_2–CeO_2 adsorbent

			C_0 (mg L^{-1})		
Models	Equation of the model	Parameters	2	5	10
Pseudo-first order	$q_t = q_e(1 - \exp(-k_1 t))$	$q_{e,exp}$(mg g^{-1})	1.3 ± 0.2	3.3 ± 0.2	6.6 ± 0.2
		$q_{e,cal}$(mg g^{-1})	1.31 ± 0.2	1.14 ± 0.5	6.42 ± 1.2
		k_1(s^{-1})	1.32 ± 0.002	1.13 ± 0.04	0.98 ± 0.004
		R^2	0.9963	0.9339	0.9845
		χ^2	0.0038	0.2333	0.0754
		MSR	0.0008	0.0926	0.0834
Pseudo-second order	$q_t = \frac{q_e^2 k_2 t}{(1+q_e k_2 t)}$	$q_{e,cal}$(mg g^{-1})	1.32 ± 0.1	3.30 ± 0.4	6.55 ± 1.4
		k_2(g mg^{-1} s^{-1})	4.56 ± 0.08	1.19 ± 0.03	0.43 ± 0.01
		R^2	0.9989	0.9986	0.9963
		χ^2	0.0011	0.0036	0.0183
		MSR	0.0002	0.0019	0.0196

Here q_e is the amount of fluoride adsorbed at equilibrium (mg g^{-1}), q_t is the quantity of fluoride adsorbed at the instant t (mg g^{-1}), k_1 is the adsorption rate constant for pseudo-first order reaction (s^{-1}), t is the contact time (s), k_2 is adsorption rate constant for the second order reaction in (g mg^{-1} s^{-1}) and $q_{e,cal}$ is the adsorption capacity calculated on the basis of the pseudo-first order and pseudo-second order equations

Table 6 Comparison of adsorption capacity with different reported adsorbents and the corresponding parameters

Adsorbents	Capacity (mg g^{-1})	pH	Contact time	References
ZrO_2-Ze	0.34	6	8 h	[34]
Cerium loaded cellulose nanocomposite bead	0.095	3	1 h	[41]
Zr–Mn composite	3.05	7	145 min	[42]
Zirconium impregnated carbon	1.83	3	180 min	[43]
Zr impregnated cellulose	4.95	4.5–5.5	50 min	[44]
SO_4^{2-}–ZrO_2–CeO_2	10.37	2–8	35 s	This work

Table 7 Isotherm model parameters and error functions data for various kinetic model for the adsorption of fluoride onto the multifunctional nano-oxide SO_4^{2-}–ZrO_2–CeO_2 adsorbent

Models	Equation of the model	Parameters	XSZC
Langmuir	$q_e = \frac{k_L q_m c_e}{(1+k_L c_e)}$	$q_{e,exp}$(mg g^{-1})	6.6 ± 0.2
		q_m(mg g^{-1})	10.4 ± 1.3
		k_L(L mg^{-1})	5.4 ± 1.5
		R^2	0.9940
		χ^2	0.0598
		MSR	0.2222
Freundlich	$q_e = K_F c_e^{1/n}$	n_F	1.74 ± 0.02
		k_F(L g^{-1})	13.1 ± 0.2
		R^2	0.9999
		χ^2	0.000006
		MSR	0.000004

Here c_e is the equilibrium concentration of fluoride (mg L^{-1}); q_e is the amount of fluoride adsorbed at equilibrium (mg g^{-1}); q_m represents the maximum adsorption capacity of fluoride on per weight of adsorbent (mg g^{-1}); k_L is the Langmuir constant related to the energy of adsorption (L mg^{-1}); k_F is the Freundlich constant related to the relative adsorption capacity of the adsorbent (L g^{-1}), and 1/n is the adsorption intensity

$$lnK_d = \frac{\Delta S^\circ}{R} - \frac{\Delta H^\circ}{RT} \tag{8}$$

Here T is the absolute temperature (K), K_d is the apparent equilibrium constant. qe is the adsorption capacity (mg g^{-1}) and R is the universal gas constant (8.314 J mol^{-1} K^{-1}).

The results were triplicated and the standard deviation was considered as the error.

The calculated thermodynamic parameters are presented in Table 4. Negative values of $\Delta_r G^\circ$ at different temperatures for SO_4^{2-}–ZrO_2–CeO_2 shows that the fluoride adsorption is spontaneous and thermodynamically favorable. The positive values of $\Delta_r S^\circ$ and $\Delta_r H^\circ$ indicate a rise in randomness at the solid–liquid interface and an endothermic adsorption process. The $\Delta_r H^\circ$ value is greater than 40 kJ mol^{-1},

suggesting a strong attractive force and a chemical nature of adsorbent–adsorbate interaction.

Adsorption kinetics

Two nonlinear kinetic models, namely the pseudo-first order and the pseudo-second order, are applied to our data for a better understanding of the mechanism of fluoride adsorption by nano-oxide SO_4^{2-}–ZrO_2–CeO_2 adsorbent. Table 5 displays the various parameters of the two kinetic models for each concentration. The kinetic graphs of these models, produced by nonlinear regression, are shown in Fig. S7. Higher R^2 values and lower χ^2 and MSR values are found to confirm the fitting of different kinetic models to the experimental data. These results imply that the adsorption proceeds with pseudo-second order kinetics, with greater values of R^2 and low values of MSR and χ^2 error functions.

At different initial fluoride concentrations, the pseudo-second order model reproduced well the experimental data, predicted adsorption capacities were found to be very close to the experimental quantities. The nano-oxide SO_4^{2-}–ZrO_2–CeO_2 adsorption capacity found in this work is compared to the adsorption capacities of several adsorbents previously reported [42–44] in the literature (Table 6).

Adsorption isotherms

The nonlinear Langmuir and Freundlich isotherms were used in the adsorption isotherm analysis. Fig. S8 displays the fitting isotherms results of these models produced by nonlinear regression, and Table 7 provides a summary of the computed parameters. A comparison of error functions shows that the Freundlich isotherm for the nonlinear form of adsorption isotherms has an excellent correlation with the experimental data for the current adsorption investigation. This isotherm yields greater values of R^2 and lower values of the MSR and χ^2 error functions. This result indicates that the Freundlich adsorption isotherm model provides a better description of the fluoride nano-oxide SO_4^{2-}–ZrO_2–CeO_2 adsorption, indicating

Table 8 Characteristics of the natural tap water sample from the city of Metlaoui (Gafsa, southern Tunisia)

Water sample	Ion content (mg L^{-1})	Tunisian potability standards (NT 09.14)	Who standards
Mg^{2+}	189.6	150	–
F^-	3.53	0.8	1.5
SO_4^{2-}	1182	600	250
Cl^-	420	600	300
HCO_3^-	189	–	–
NO_3^-	18.39	45	50
Na^+	337	200	200
Ca^{2+}	232	300	500

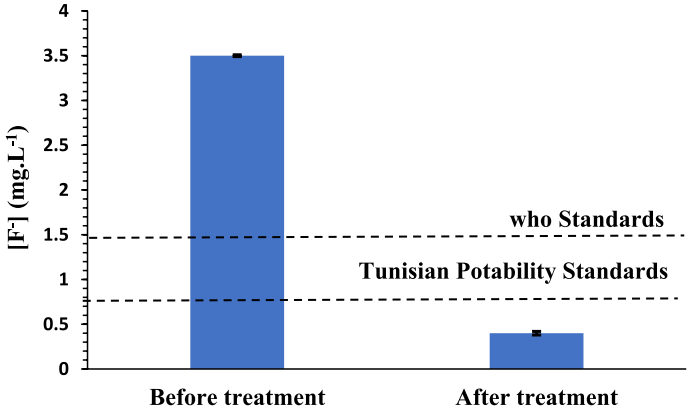

Fig. 10 Concentration of fluoride in sample water before and after treatment by multifunctional nano-oxide SO_4^{2-}–ZrO_2–CeO_2 adsorbent

that multi-layer adsorption was the adsorption process. The obtained n_F values were greater than unity, indicating that the fluoride adsorption was favorable.

Removal fluoride from real sample by SO_4^{2-}–ZrO_2–CeO_2 material

The fluoride in the drinking tap water sample from Metlaoui, Gafsa, in southern Tunisia, is eliminated using our adsorption process, under optimal conditions, (pH 7, m = 30 mg, Contact time = 35 s, T = 25 °C). The physico-chemical analysis of the water before treatment is displayed in Table 8. This natural water presents a high fluoride concentration (3.53 mg L^{-1}) exceeding the limit, recommended by the WHO (1.5 mg L^{-1}) and by Tunisian potability standards (NT 09.14) (0.8 mg L^{-1}).

After treatment of water sample by XSZC adsorbent (Fig. 10), the fluoride concentration was reduced (0.40 mg L^{-1}) bellow the standards, even in complex matrix. This outcome demonstrated the potential utility of our multifunctional nano-oxide adsorbent for fluoride removal in water treatment applications.

Conclusion

A series of bimetallic ZrO_2–CeO_2 nano-oxide adsorbents with different Ce/Zr molar ratios were produced by sol–gel in one step to find the optimal ZrO_2–CeO_2 composition for fluoride removal. The ideal ZrO_2–CeO_2 (Ce/Zr = 0.3) adsorbent was functionalized by sulfate groups and then applied to remove fluoride from drinking water. Our results reveal that at neutral pH and ambient temperature, the resultant multifunctional nano-oxide SO_4^{2-}–ZrO_2–CeO_2 shows a high removal rate reaching 100% without any additional treatment steps. The outstanding fluoride removal ability of the SO_4^{2-}–ZrO_2–CeO_2 nanoparticle is attributed to its mesoporous structure,

and its large specific surface area (more than 200 $m^2\ g^{-1}$). Additionally, the simultaneous existence of sulfate anions and superficial hydroxyl groups on XSZC's surface justifies the adsorbent's tremendous potential in the defluoridation of drinking water. FTIR analysis and pH studies confirmed that the adsorption mechanism is due to electrostatic attraction and ligand exchange. Because of its rapid extraction kinetics (contact time at equilibrium < 1 min), high desorption characteristics, recyclability, and application in a wide pH range (2–8) at a very low adsorbent dose (30 mg), the SO_4^{2-}–ZrO_2–CeO_2 adsorbent is a promising adsorbent for fluoride removal. In Tunisia, where the population is obviously impacted by the gradual onset of fluorosis, this defluoridation procedure is highly advantageous for the treatment of drinking water. Our adsorption process, can easily used in rural areas in Tunisia. Apart from being effective, this Zr-Ce-based adsorption technology has the environmental benefit of being less harmful than other materials requiring extensive energy-intensive processing.

Supplementary Information The online version contains supplementary material available at https://doi.org/10.1007/s11144-024-02681-3.

Acknowledgements The financial support for this work was provided by the national project PEJC (Project PEJC2023-D1P11), Ministry of Higher Education and Scientific Research of Tunisia.

Funding Ministère de l'Enseignement Supérieur et de la Recherche Scientifique, Projet PEJC 2023-D1P11, Nesrine Kamoun.

Data availability The dataset generated and /or analyzed during the current study are available from the corresponding author on reasonnable request.

References

1. Karmakar S, Bhattacharjee S, De S (2018) Aluminium fumarate metal organic framework incorporated polyacrylonitrile hollow fiber membranes: spinning, characterization and application in fluoride removal from groundwater. J Chem Eng 334:41–53
2. Guissouma W, Hakami O, Al-Rajab AJ, Tarhouni J (2017) Risk assessment of fluoride exposure in drinking water of Tunisia. Chemosphere 177:102–108
3. World Health Organization (2017) Guidelines for Drinking-Water Quality, 4th ed incorporating the 1st addendum
4. Kumar P, Kumar M, Barnawi AB, Maurya P, Singh S, Shah D, Yadav VK, Kumar A, Kumar R, Yadav KK, Gacem A, Ahmad A, Patel A, Alreshidi MA, Singh V, Yaseen ZM, Cabral-Pinto MMS, Vinayak V, Wanale SG (2024) A review on fluoride contamination in groundwater and human health implications and its remediation: a sustainable approaches. Environ Toxicol Pharmacol 106:104356
5. Trikha R, Sharma BK (2014) Studies on factors affecting fluoride removal from water using passive system. J Environ Chem Eng 2(1):172–176
6. Waghmare SS, Arfin T (2015) Fluoride removal from water by various techniques: review. Int J Innov Sci Eng Technol 2(9):560–571
7. Shen J, Schäfer A (2014) Removal of fluoride and uranium by nanofiltration and reverse osmosis: a review. Chemosphere 117:679–691
8. Sandoval MA, Fuentes R, Nava JL, Rodríguz I (2014) Fluoride removal from drinking water by electrocoagulation in a continuous filter press reactor coupled to a flocculator and clarifier. Sep Purif Technol 134:163–170

9. Dar FA, Kurella S (2023) Recent advances in adsorption techniques for fluoride removal—an overview. Groundw Sustain Dev 23:101017
10. Singh K, Lataye DH, Wasewar KL (2017) Removal of fluoride from aqueous solution by using bael (*Aegle marmelos*) shell activated carbon: kinetic, equilibrium and thermodynamic study. J Fluor Chem 194:23–32
11. Patra G, Das P, Chakraborty S, Meikap BC (2018) Removal of fluoride from wastewater using HCl-treated activated alumina in a ribbed hydrocyclone separator. J Environ Sci Heal A 53:1–8
12. Grybos M, Billard P, Desobry-Banon S, Michot LJ, Lenain JF, Mustin C (2011) Bio-dissolution of colloidal-size clay minerals entrapped in microporous silica gels. J Colloid Interf Sci 362:317
13. Sun Y, Fang Q, Dong J, Cheng X, Jiaqiang X (2011) Removal of fluoride from drinking water by natural stilbite zeolite modified with Fe (III). Desalination 277:121–127
14. Wajima T, Umeta Y, Narita S, Sugawara K (2009) Adsorption behavior of fluoride ions using a titanium hydroxide derived adsorbent. Desalination 249:323–330
15. Khandare D, Mukherjee S (2019) A Review of Metal oxide Nanomaterials for Fluoride decontamination from Water Environment. Mater Today: Proc 18:1146–1155
16. Savari A, Hamidi A, Farjadfard S, Omidvar M, Ramavandi B (2023) Zirconium-based materials for fluoride removal from aqueous environments: a literature review and scientometric analysis. Colloid and Interface Science Communications 55:100722
17. Kamoun N, Mezghich S, Mansour L, Younes MK, Elfil H (2022) Characteristic and adsorption properties of zirconia aerogel and xerogel nanostructure application to fluoride removal from drinking water of Tunisian south region. Desalin Water Treat 268:170–181
18. Kahya N, Erim FB (2023) Removal of fluoride ions from water by cerium-carboxymethyl cellulose beads doped with CeO_2 nanoparticles. Int J Biol Macromol 242:124595
19. Zhu BS, Jia Y, Jin Z, Sun B, Luo T, Yu XY, Kong LT, Huang XJ, Liu JH (2015) Controlled synthesis of natroalunite microtubes and spheres with excellent fluoride removal performance. Chem Eng J 271:240–251
20. Jia Y, Zhu BS, Zhang KS, Jin Z, Sun B, Luo T, Yu XY, Kong LT, Liu JH (2015) Porous 2-line ferrihydrite/bayerite composites (LFBC): fluoride removal performance and mechanism. Chem Eng J 268:325–336
21. Chai LY, Wang YY, Zhao N, Yang WC, You XY (2013) Sulfate-doped Fe_3O_4/Al_2O_3 nanoparticles as a novel adsorbent for fluoride removal from drinking water. Water Res 47:4040–4049
22. Yu Y, Yu L, Chen JP (2015) Adsorption of fluoride by Fe–Mg–La triple-metal composite: adsorbent preparation, illustration of performance and study of mechanisms. Chem Eng J 262:839–846
23. Chen L, Zhang KS, He JY, Xu WH, Huang XJ, Liu JH (2016) Enhanced fluoride removal from water by sulfate-doped hydroxyapatite hierarchical hollow microspheres. Chem Eng J 285:616–624
24. Ksila W, Younes MK, Ghorbel A, Rives A (2021) Characterization and catalytic reactivity of xerogel catalysts based on mesoporous zirconia doped with telluric acid prepared by sol–gel method: mechanistic study of acetic acid esterification with benzyl alcohol. J Sol-Gel Sci Technol 99:376–390
25. Langmuir I (1918) The adsorption of gases on plane surfaces of glass, mica and platinum. J Am Chem Soc 40:1361–1403
26. Gabor L (2015) Deterministic kinetics in chemistry and systems biology: the dynamics of complex reaction networks. Springer, Cham
27. Freundlich HMF (1906) Über die Adsorption in Lösungen. Z Phys Chem 57:385–470
28. Thommes M, Kaneko K, Neimark AV, Olivier JP, Reinoso RF, Rouquerol J, Sing KSW (2015) Physisorption of gases, with special reference to the evaluation of surface area and pore size distribution (IUPAC technical report). Pure Appl Chem 87:1051–1069
29. Korde S, Tandekar S, Jugade RM (2020) Novel mesoporous chitosan-zirconia-ferrosoferric oxide as magnetic composite for defluoridation of water. Environ Chem Eng 8:104360
30. Sun Y, Ma S, Du Y, Yuan L, Wang S, Yang J, Deng F, Xiao FS (2005) Solvent-free preparation of nanosized sulfated zirconia with brønsted acidic sites from a simple calcination. J Phys Chem B 109:2567–2572
31. Patel SB, Panda AK, Swain SK, Patnaik T, Muller F, Delpeux-Ouldriane S, Duclaux L, Dey RK (2018) Development of aluminum and zirconium based xerogel for defluoridation of drinking water: study of material properties, solution kinetics and thermodynamics. J Environ Chem Eng 6:6231–6242

32. Yu Z, Xu C, Yuan K, Gan X, Feng C, Wang X, Zhu L, Zhang G, Xu D (2018) Characterization and adsorption mechanism of ZrO_2 mesoporous fibers for health-hazardous fluoride removal. J Hazard Mater 346:82–92
33. Zhang G, Qu J, Liu H, Liu R, Wu R (2007) Preparation and evaluation of a novel Fe-Mn binary oxide adsorbent for effective arsenite removal. Water Res 41:1921–1928
34. Gao Y, Li M, Ru Y, Fu J (2021) Fluoride removal from water by using micron zirconia/zeolite molecular sieve: Characterization and mechanism. Groundw Sustain Dev 13:100567
35. He J, Chen JP (2014) A zirconium-based nanoparticle: essential factors for sustainable application in treatment of fluoride containing water. J Colloid Interface Sci 416:227–234
36. Kamoun N, Younes MK, Ghorbel A, Mamède AS, Rives A (2014) Effect the solvent evacuation mode on the catalytic properties of nickel-modified sulfated zirconia catalysts: n-hexane isomerization. Reac Kinet Mech Cat 111:199–213
37. Gosh A, Chakrabarti S, Biswas K, Gosh UC (2014) Agglomerated nanoparticles of hydrous Ce (IV) and Zr (IV) mixed oxide: preparation, characterization and physicochemical aspects on F^- adsorption. Appl Surf Sci 307:665–676
38. Chigondo M, Paumo HK, Bhaumik M, Pillay K, Maity A (2018) Rapid high adsorption performance of hydrous cerium magnesium oxides for removal of fluoride from water. J Mol Liq 265:496–509
39. Swain SK, Patnaik T, Singh VK, Jha U, Patel RK, Dey RK (2011) Kinetics, equilibrium and thermodynamic aspects of removal of fluoride from drinking water using meso-structured zirconium phosphate. Chem Eng J 171:1218–1226
40. Dou X, Zhang Y, Wang H, Wang T, Wang Y (2011) Performance of granular zirconium-iron oxide in the removal of fluoride from drinking water. Water Res 45(12):3571–3578
41. Santra D, Joarder R, Sarkar M (2014) Taguchi design and equilibrium modeling for fluoride adsorption on cerium loaded cellulose nanocomposite bead. Carbohyd Polym 111:813–821
42. Tomar V, Prasad S, Kumar D (2013) Adsorptive removal of fluoride from water samples using Zr–Mn composite material. Microchem J 111:116–124
43. Alagumuthu G, Rajan M (2010) Equilibrium and kinetics of adsorption of fluoride onto zirconium impregnated cashew nut shell carbon. Chem Eng J 158:451–457
44. Barathi M, Kumar ASK, Rajesh N (2014) A novel ultrasonication method in the preparation of zirconium impregnated cellulose for effective fluoride adsorption. Ultrason Sonochem 21:1090–1099